SPECIAL FOCUS: BRIDGE INNOVATIONS

Development and Experimental Testing of Connections for the Simple for Dead Load–Continuous for Live Load Steel Bridge System

NICK LAMPE, NAZANIN MOSSAHEBI, AARON YAKEL, REZA FARIMANI and ATOROD AZIZINAMINI

ABSTRACT

The most critical aspect of the simple for dead load and continuous for live load (SDCL) bridge system is identifying a detail capable of connecting the girders over the interior supports. An experimental program was set up to identify and study the fundamental characteristics of an interior connection for the SDCL bridge system. Three full-scale test specimens were constructed and tested, each using different connection details for possible use in the SDCL bridge system. Each specimen was subjected to two types of loading: cyclic testing to simulate long-term truck traffic loads and an ultimate load test to determine the ultimate capacity of the system. Results of the tests indicated that connection details meeting the design provisions could consist of embedding the girder ends in the concrete diaphragm and would provide a good service life. The main objective in using a concrete diaphragm to join the girder ends over the interior support is to prevent crushing of the concrete adjacent to the compression flanges of the girder and embedded in the concrete diaphragm. Two of the primary conclusions are that deck reinforcement is sufficient to develop continuity and the top flange need not be continuous over the interior support.

Keywords: steel bridges, steel girders, SDCL, simple for dead load–continuous for live load.

INTRODUCTION

The simple for dead load and continuous for live load (SDCL) bridge system utilizes a joint detail at the interior supports that does not become continuous until after the dead loads have been applied. Prior to attaining final continuity, the girders within the individual spans are simply supported. General information regarding the behavior and design of the SDCL system can be found in Azizinamini (2014).

To study potential details that could be used over interior supports of SDCL bridge systems, three full-scale specimens were tested. The design and construction of each specimen was completed according to the second edition of the American Association of State Highway and Transportation Officials (AASHTO) *Load and Resistance Factor Design Specifications* (AASHTO, 1998). Specimen 1 was intended to be a proof-of-concept specimen utilizing a connection detail that had a high probability of success. The purpose of specimen 2 was to explore the failure mechanisms that developed utilizing a minimalist connection detail. This provided a baseline and indicated what modes of failure needed to be addressed. Specimen 3 utilized a modified detail similar to that used in specimen 1 but simpler to construct and implement. In order to represent the loads that the structure would encounter, each specimen was subjected to two types of loading: cyclic testing to simulate long-term truck traffic loads and an ultimate load test to determine the ultimate capacity of the system.

DESIGN OF SPECIMENS

The prototype for the test specimens consisted of an existing in-service bridge. The prototype bridge is a two-span continuous structure, with each span 95 ft long and designed based on AASHTO LRFD specifications (1998). Detailed design of the prototype bridge is provided in Lampe (2001).

The test specimens represent the interior pier region of the two-span bridge, approximately from point of inflection to point of inflection centered about interior pier, as shown in Figure 1. Loads applied at the ends of the cantilevers allowed simulation of the type of loading the structure would be subjected to in the field and result in similar shear and moment profiles.

Nick Lampe, P.E., Bridge Engineer, HDR Engineering, Inc., Omaha, NE. E-mail: nick.lampe@hdrinc.com

Nazanin Mossahebi, Project Manager, Bureau Veritas North America, Inc., Los Angeles, CA. E-mail: nmossahebi@dpw.lacounty.gov

Aaron Yakel, Ph.D., Research Associate, Civil and Environmental Engineering Department, Florida International University, Miami, FL. E-mail: ayakel@fiu.edu

Reza Farimani, Ph.D, P.E., LEED AP, Associate, Thornton Tomasetti, New York, NY. E-mail: rfarimani@thorntontomasetti.com

Atorod Azizinamini, Ph.D., P.E., Professor and Chair, Civil and Environmental Engineering Department, Florida International University, Miami, FL (corresponding). E-mail: aazizina@fiu.edu

SPECIMEN DETAILS

The basic geometry and reinforcing are similar for all test specimens and are presented first. The specific differences in the connection details for each specimen are then presented. Figure 1 shows the basic geometry of the test specimens.

Concrete Diaphragm

The detailing of the diaphragm was similar to standard details used by many state departments of transportation. Reinforcement of the diaphragm consisted of closed #5 hoops spaced at 12 in. and #5 bars along the transverse faces. Holes were provided in the webs of the steel girders to allow the transverse reinforcement to pass through. A schematic of the diaphragm is shown in Figure 2.

Deck Reinforcement

The reinforcement of the 7½-in.-thick deck was based on the empirical deck design provisions given in the AASHTO LRFD specifications (AASHTO, 1998). The longitudinal steel includes #5 bars at 12 in. on center in the top layer and #4 bars at 12 in. on center in the bottom layer. The transverse reinforcement consists of #5 bars at 12 in. on center in the bottom layer and #4 bars at 12 in. on center in the top layer.

The negative moment produced by the live loads and superimposed dead loads are resisted by additional slab reinforcement at the interior pier location. One purpose of the larger research project was to determine any special requirements for this additional continuity reinforcement. Therefore, as a starting point, design of longitudinal rebar for the experimental program utilized classical concrete design theory. The details of calculations can be found in Lampe (2001). Based on this method, the additional reinforcement required in the top layer is comprised of two #8 bars centered between adjacent #5 bars. Similarly, one #7 bar is centered between adjacent #4 bars in the bottom longitudinal layer. This follows the AASHTO section 6.10.1.7 requirement of having ⅔ of the reinforcing steel in the top layer and ⅓ of the total area in the bottom layer. The details of the final slab reinforcement are shown in Figure 3.

Girder Connection Details

Three specimens were tested, each having different beam end connection details. This section provides description of different beam end details tested. The objective of test 1 was to examine a girder end detail with high probability of acceptable performance. In specimen 1, an end bearing plate is welded to the end of the girder (see Figure 4a). Two triangular plates are added to stiffen the end bearing plate above the bottom flange. The main characteristic of this specimen is the continuity of the bottom flanges over the pier. This continuity ensures that the specimen is capable of transferring the compressive stress of the bottom flange without substantial crushing of the diaphragm concrete. The connection of the two girders was done by extending the bottom flange plates and welding them together with complete-joint-penetration groove welds. This particular detail

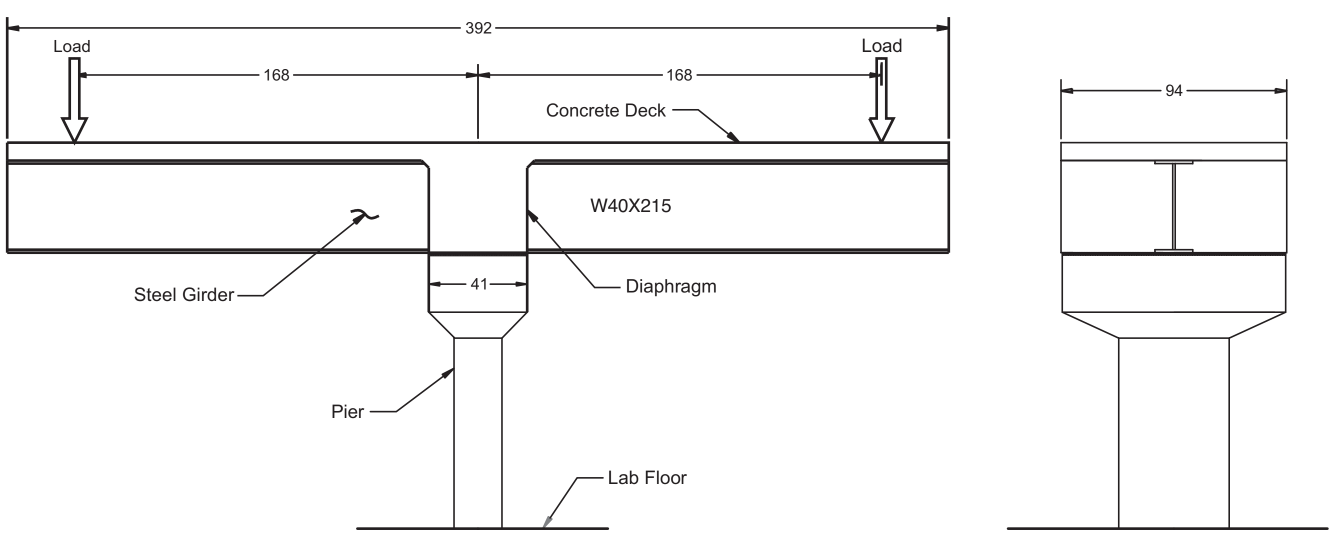

Fig. 1. Conceptual test specimen, dimensions in inches.

is certainly not considered cost effective, especially when conducted in the field. However, the goal of test 1 was to provide proof of concept. Later specimens then began to address cost effectiveness of the detailing.

The objective of test 2 was to establish the baseline and determine if special details at the girder ends are required. In specimen 2, the two girders simply sit on the pier, and the concrete diaphragm confines them (see Figure 4b). The two girders are completely separated, and there is no connection between bottom flanges. The negative moment is transferred through composite action of concrete and steel in the diaphragm. More complete information about specimen 2 can be found in Mossahebi (2004).

Test 3 was developed after completion of tests 1 and 2. The detail used in specimen 1 was judged to be acceptable, while the detail used in specimen 2 was judged to be unacceptable. The objective of specimen 3 was to explore the possibility of using a simpler form of the details used in specimen 1. Specimen 3 utilized bearing plates (without triangular stiffener plates) welded to the ends of the girders similar to specimen 1, but the bottom flanges were not connected (see Figure 4c). There was an 8-in. gap between the two girders.

CONSTRUCTION AND ERECTION

Construction of each test specimen was completed in the structures laboratory at the University of Nebraska–Lincoln. A reinforced concrete pier was built to support the cantilever system for all three specimens. The girders for the specimens were cut from the same stock (W40×215 rolled I-girders). A 15.75-in.-wide by 36-in.-long by 1-in.-thick 80-durometer elastomeric bearing was placed on the pier for the girders to bear on. Polystyrene 1 in. thick was placed at the base of the diaphragm to prevent bonding between the pier and concrete diaphragm and allow the girder rotation. Dowel bars were also provided as shown in Figure 5.

The combined details used allow rotation of the girders about the pier centerline while preventing the horizontal translation of the girders.

After the girders were set, diaphragm-reinforcing steel was placed and embedment gages were set. Formwork for the deck and diaphragm was added after the diaphragm-reinforcing steel was placed. Once the deck formwork was completed, the diaphragm was partially cast to approximately ¾ the height of the web to stabilize the specimens prior to casting of the deck. Once the diaphragm was poured, deck reinforcement was placed. The concrete deck was cast three days after the diaphragm was cast.

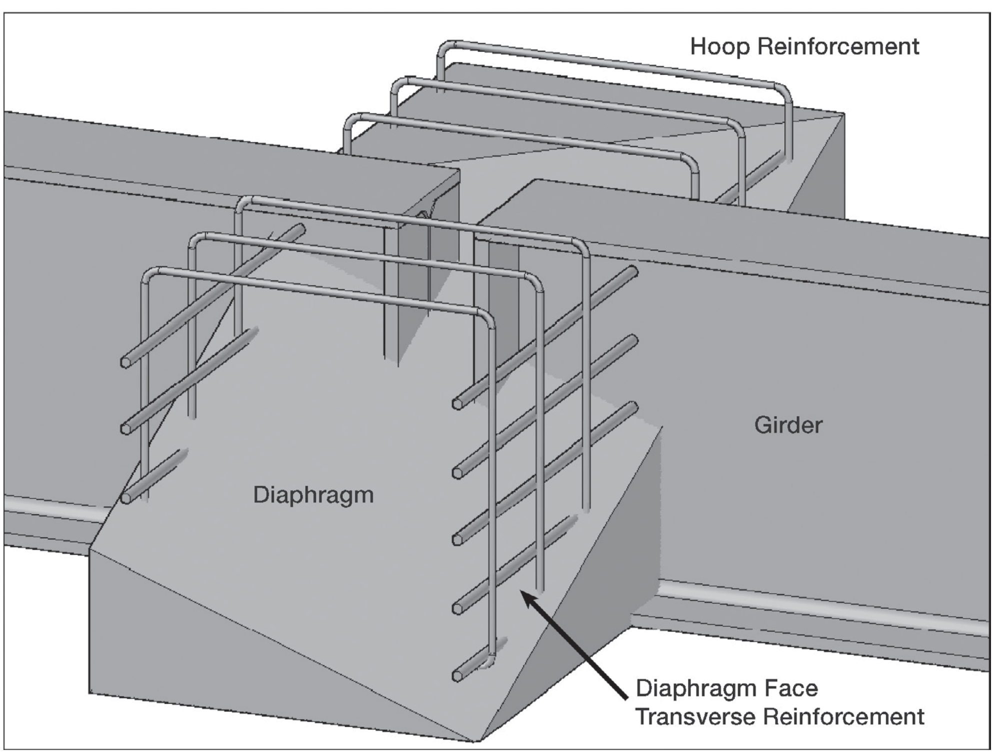

Fig. 2. Concrete diaphragm detail (cutaway).

INSTRUMENTATION

Several types of instrumentation were used to monitor performance of the test specimens under applied loads. Instruments included electrical strain gages, vibrating wire embedment gages and potentiometers. The strain gages were mounted on the steel girders and reinforcing bars. The embedment gages were placed inside the concrete diaphragm and deck. The potentiometers were used to measure the displacement of the end of the cantilevers. The horizontal movement of the bottom flanges into the diaphragm was measured by a potentiometer in specimen 3. To apply load on the specimens, displacement was applied at the end of each cantilever by hydraulic rams. The pressure of hydraulic oil inside the rams was measured by pressure meters built into the rams. Complete details of the instrumentation can be found in the experimentation report (Azizinamini et al., 2005).

MATERIAL PROPERTIES

The laboratory test specimens were constructed using materials representative of those utilized in typical bridge construction. Several component tests were performed in order to ensure that the bridge components possessed the specified material properties. The deck slab and diaphragm concrete had a specified minimum compressive strength of 4000 psi and were reinforced with grade 60 reinforcing bars. The bridge girders were fabricated from W40×215 rolled I-girders conforming to ASTM A709-50W specifications. The material testing procedure and results for each specimen are presented in the following sections.

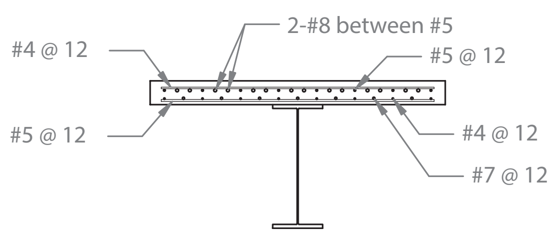

Fig. 3. Concrete slab section.

Concrete

For concrete, several 6-in.-diameter by 12-in.-long concrete cylinder samples were taken during the casting of both the diaphragm and the deck. The average compressive strength of cylinder specimens, tested in accordance with ASTM C39, is shown in Table 1.

Reinforcement Steel

For the steel reinforcing materials, samples of each deck-reinforcing-bar size were tested. Each sample was tested as a full section according to ASTM A370 specifications. Results of the tensile test are given in Table 2. The average reinforcing-bar yield stress was approximately 65 ksi for test 1, 73 ksi for test 2 and 69 ksi for test 3.

Girder Steel

Four material samples were taken from specimen 1, two each from the web and flange. The samples were taken from regions that were subjected to low flexural stresses during the testing sequence. The samples were tested as full sections according to the ASTM A370 specifications. The average yield strength of the girder steel was determined to be

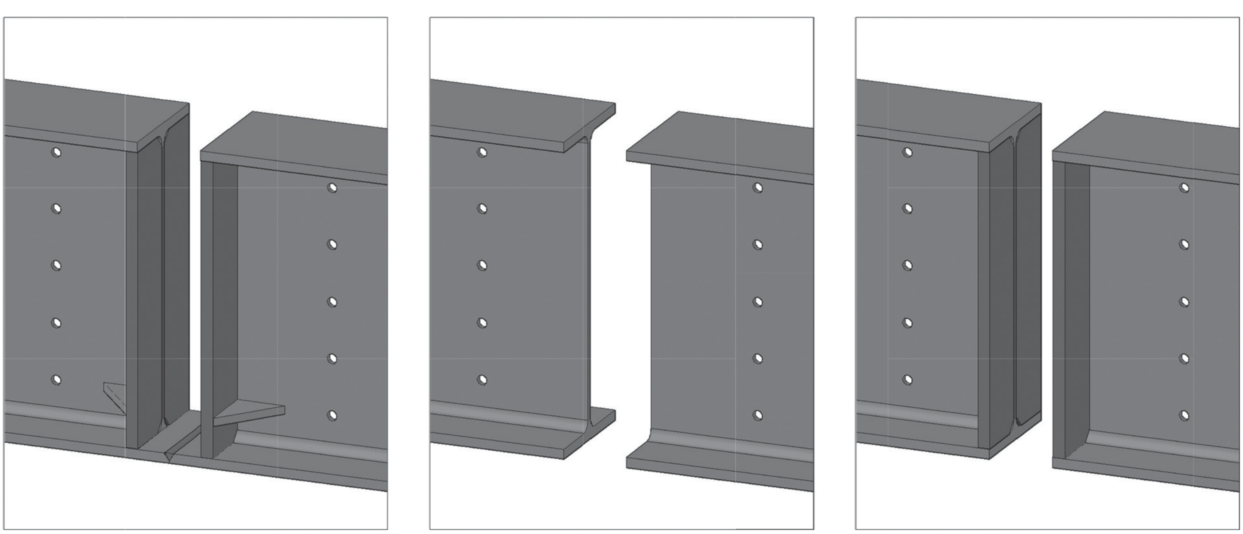

Fig. 4. Details of test specimens inside the diaphragm: (a) specimen 1; (b) specimen 2; (c) specimen 3.

Table 1. Average Concrete Compressive Strength, f'_c		
Test	f'_c (ksi)	
	Slab	Diaphragm
1	4.98	6.26
2	5.45	7.14
3	7.24	5.89

Table 2. Reinforcement Tensile Test Results							
Bar Size	Yield Strength, f_y (ksi)			Ultimate Strength, v_u (ksi)			f_u/f_y
	Test 1	Test 2	Test 3	Test 1	Test 2	Test 3	
#4	64.2	71.5	70.3	101.0	114.2	113.4	1.57
#5	63.8	76.5	68.9	101.0	122.8	108.7	1.58
#7	68.2	67.5	64.3	101.0	109.5	104.6	1.48
#8	65.5	75.5	73.2	105.4	110.6	107.8	1.61

Fig. 5. Photo of the two girders during construction.

57 ksi, and the average ultimate stress was 72 ksi. The material from all three specimens came from the same stock and separate material tests were not performed on specimens 2 and 3.

CYCLIC TESTING

The bridge structure is expected to endure millions of cycles of repeated axle loads from vehicles during the design life. The available data show that the number of trucks on a bridge can reach more than 180 million vehicle load cycles during the lifetime of 100 years (Szerszen and Nowak, 2000). The proposed connection should be able to operate and survive when subjected to cyclic loading generated by truck traffic. The specific goal of the cyclic testing performed was not intended to determine the fatigue strength or limit of the details, but rather as a proof loading to investigate whether the proposed details are capable of surviving a loading regimen equivalent to the cyclic loading anticipated over the design life of the bridge.

Cyclic Testing Procedures

The fatigue limit state load combination was used to calculate the shear and moment envelope to which the prototype bridge would be subjected to. According to AASHTO LRFD specifications (1998), during its 75-year design life, the prototype bridge (and, consequently, the connection of the two girders at the pier location) will experience 135,000,000 cycles of truck loadings. The simulation of this number of cycles in the laboratory would have taken a prohibitively long time. Therefore, there was a need to develop a procedure that could simulate 75 years of traffic in a reasonable time frame. Following is a discussion of the procedure that was used during the cyclic loading tests that allowed for a reduction in the number of cycles by increasing the magnitude of the applied load.

The connection detail is composed of steel and concrete elements in a complex arrangement, and there is no single fatigue life model that applies to situation. Therefore, at the outset, it was assumed that the steel elements within the detail would control the fatigue life of the detail; consequently, the fatigue model for steel, given by Equation 1, was used to determine the amplified load. In this expression, A is a constant dependent upon the geometry and the detail under consideration, while the exponent ⅓ is characteristic for the material and is the slope (negative) of the stress versus number of cycles curve when plotted on log-log scales. Regardless of the value of A, which is unknown for the detail under consideration, the fatigue model can be used to determine the amplified loading value.

$$\Delta F\left(\frac{A}{N}\right)^{1/3} \tag{1}$$

where:

N = number of cycles to failure
A = a constant representing the detail category of the connection
ΔF = load increment

Equation 1 may be rewritten for two conditions. Equation 2a represents the loading and number of cycles applied during the service life of the real structure as assumed for design. Equation 2b represents the structure under amplified loading.

$$M_1\left(\frac{A}{N_1}\right)^{1/3} \tag{2a}$$

$$M_2\left(\frac{A}{N_2}\right)^{1/3} \tag{2b}$$

where

M_1 = actual load
N_1 = cycles for actual structure corresponding to load of M_1
M_2 = amplified load (desired quantity)
N_2 = number of test cycles at load of M_2

Dividing M_1 by M_2 causes the constant A to cancel and results in Equation 3, which can be used to determine the amplified load M_2 that must be applied corresponding to a desired number of cycles. For the testing performed, the resulting amplified load was approximately four times nominal value.

$$\frac{M_1}{M_2} = \left(\frac{N_2}{N_1}\right)^{1/3} \tag{3}$$

If the specimen is subjected to the specified cycles at the amplified load level and does not experience a fatigue failure, the conclusion is that a fatigue failure due to the actual truck loading would occur beyond the service life of the bridge. In cases where the load intensity varied throughout the testing, Miner's rule was used to assess the cumulative damage.

The test setup had the same configuration for all three specimens. The cyclic load was applied using 220-kip hydraulic actuators placed at the ends of each cantilever as shown in Figure 6. The cyclic loading frequency was set at two cycles per second. At the beginning of each day, prior to the start of applying fatigue loads, the specimen was subjected to five cycles at a lower frequency. On the first of the five slow cycles, the specimen was held at the peak end load and data were collected from all instruments, including the embedment gages. During the application of the five slow cycles, data from all instruments except embedment gages were collected.

Displacement control was used throughout the course of the cyclic investigation. Once the stiffness was obtained, the displacement required for a desired load was calculated and then applied. In all cases, a small positive bias was imposed to prevent load reversal in the test apparatus. In test 1, the load applied at each end cycled between 2 and 106 kips. This load was applied successfully to the specimen for 2,000,000 cycles.

The same initial process was used for specimen 2, and due to a slightly different initial stiffness, the target end load was found to be 104 kips rather than 106 kips. However, after applying a few cycles, it became apparent that the specimen could not resist the desired end load of 104 kips. The maximum load achieved from the calculated displacement, based on initial stiffness, had decreased to approximately 74 kips. As a result, the number of applied loading cycles had to be increased to compensate for the lower load level. The intent of specimen 2, which was to observe the failure modes in absence of any special detailing, made it perform poorly during the cyclic testing at the amplified load levels. Recall that the load level was amplified to allow application of a lower number of cycles. The applied displacement had to be adjusted three times during the cycling load test because the load achieved at the set displacement decreased over time. The cyclic testing was terminated after applying approximately 2,780,000 cycles because the load-carrying capacity continued to deteriorate.

Based on the experience of specimen 2, it was decided to initially apply a smaller amount of load and observe the behavior of specimen 3. Therefore, the end load was set to approximately 70 kips and 2,000,000 cycles were run with this configuration. Once completed, the load was increased to 85 kips for an additional 3,515,516 cycles. The number of cycles and load range in each test are summarized in Table 3.

Fig. 6. Specimen 1 cycling test setup and fixtures.

Table 3. Number of Cycles and Load Range for the Three Specimens		
Test	**Cycles**	**Load Range (kips)**
1	2,000,000	104
2	2,780,000	74
3	5,515,516	70 and 85

Cyclic Test Results

The following is a summary of observations made during the cyclic testing and the results obtained from the instrumentation. Additional information can be found in the full reports (Azizinamini, Lampe and Yakel, 2003; Azizinamini et al., 2005).

Cracking Patterns

For all three specimens, cracks on the surface of the deck slab were documented prior to application of fatigue cycles and then again at various times during the testing. The loads applied during the cyclic test were magnified by a factor of approximately 4 to shorten the length of time required for testing. As a result of the magnification, cracking of the concrete was exacerbated, and the degree of the observed cracking is not an indication of the performance under service load.

In test 1, mapping of deck cracks was done at 1 million, 1.5 million and 2 million cycles of load. The largest crack widths were observed to occur at the face of the diaphragm, near the edge of the slab. This can be attributed to the abrupt change in rigidity due to the presence of the concrete diaphragm at the pier. Additional cracks were observed but diminished in size and frequency as one moved away from the diaphragm. A crack map for 1.5 million loading cycles is shown in Figure 7. A comparison of the crack widths at 1.5 million compared to 1 million load cycles shows that there was virtually no change in crack widths over this interval. There were a few additional short cracks propagating inward from the edge of the deck, but the measured widths of existing cracks were unchanged. The fact that the crack widths were stable was an indication that no progressive damage occurred during the course of cycling. The cracking patterns and behavior of specimen 3 was nearly identical to that of specimen 1.

In specimen 2 cracks formed through the depth of the deck over the pier and close to the edge of the diaphragm during the cyclic testing similar to specimens 1 and 3. The initial cracks were observed near the diaphragm edge. As

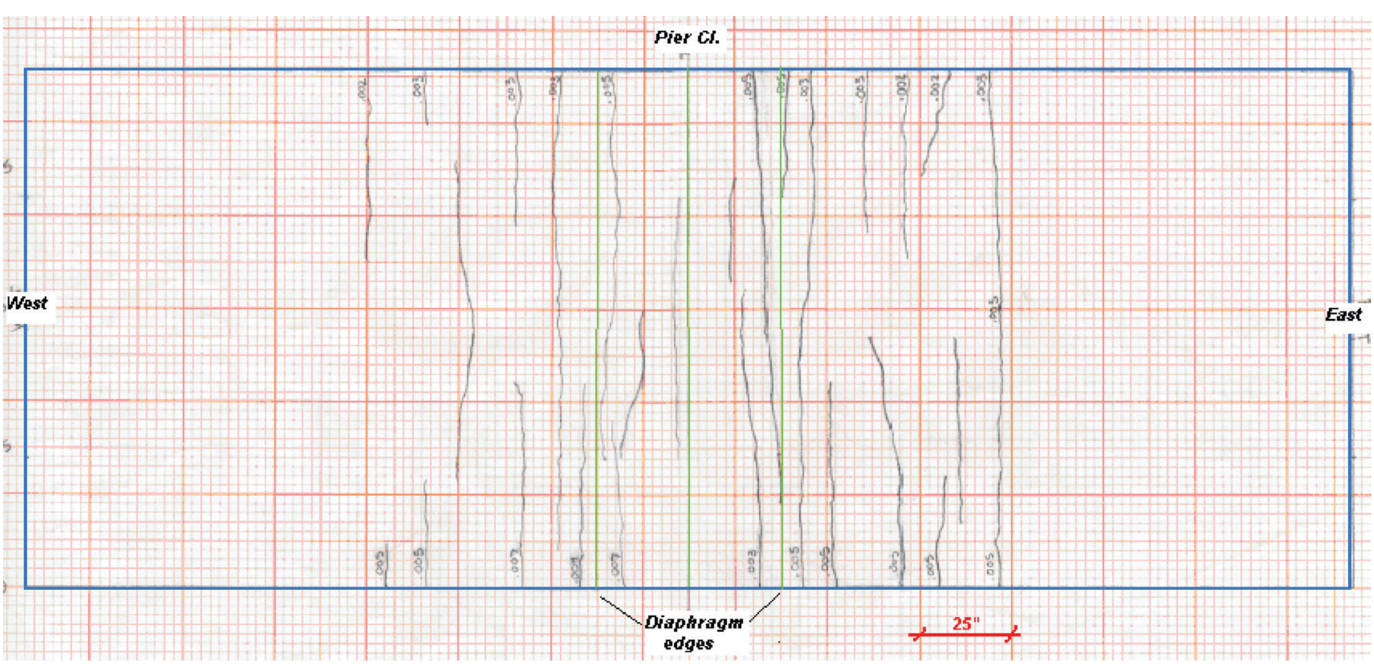

Fig. 7. Cracks mapped from the test 1 slab after 1.5 million cycles.

cyclic loading continued, the bottom flanges, subject to compression, were observed to actually penetrate into the diaphragm. This observation led to the discontinuation of testing as it had become apparent that the model was experiencing an ultimate strength failure.

Load-Deflection

The load-deflection plots shown in Figure 8 were generated from data collected from several cycles at the start of the test and then again at the end of the test. For specimen 1 (test 1), little change in stiffness was observed over the complete interval. In specimen 2 (test 2), the maximum load continued to decrease over the duration of the test. In specimen 3 (test 3), during the first 2,000,000 cycles, each day the cycling loads resulting from the applied displacement would experience a downward shift downward of nearly 10 kips by the end of the day's cycling. Note that both endpoint loads experienced the same drop so that the cycling range remained unchanged. The following day, the loads had recovered to the previous day's starting values. The effect stabilized within several hours, and on occasions when cycling was continued overnight for a period of days, there was no progressive decrease. Although no instrumentation was present to quantify the observation, the temperature of the concrete in the vicinity of the bottom flange was noticeably higher after cycling. Observation of the system stiffness, discussed in the next section, further supports the contention that the effect was due to benign causes and not fundamental structural changes.

Stiffness Softening

In specimen 1 (test 1), the experimental displacement required to attain the 106-kip load was 0.3083 in., based on the finite element analysis of the specimen under this load (Lampe, 2001). Only once was the applied displacement adjusted to maintain the 106-kip load during the cycling test. After 7400 cycles, the applied displacement was increased from 0.3083 in. to 0.3115 in. to compensate for the stiffness reduction. The amount of adjustment was about 0.5% of the initial applied displacement. The stiffness

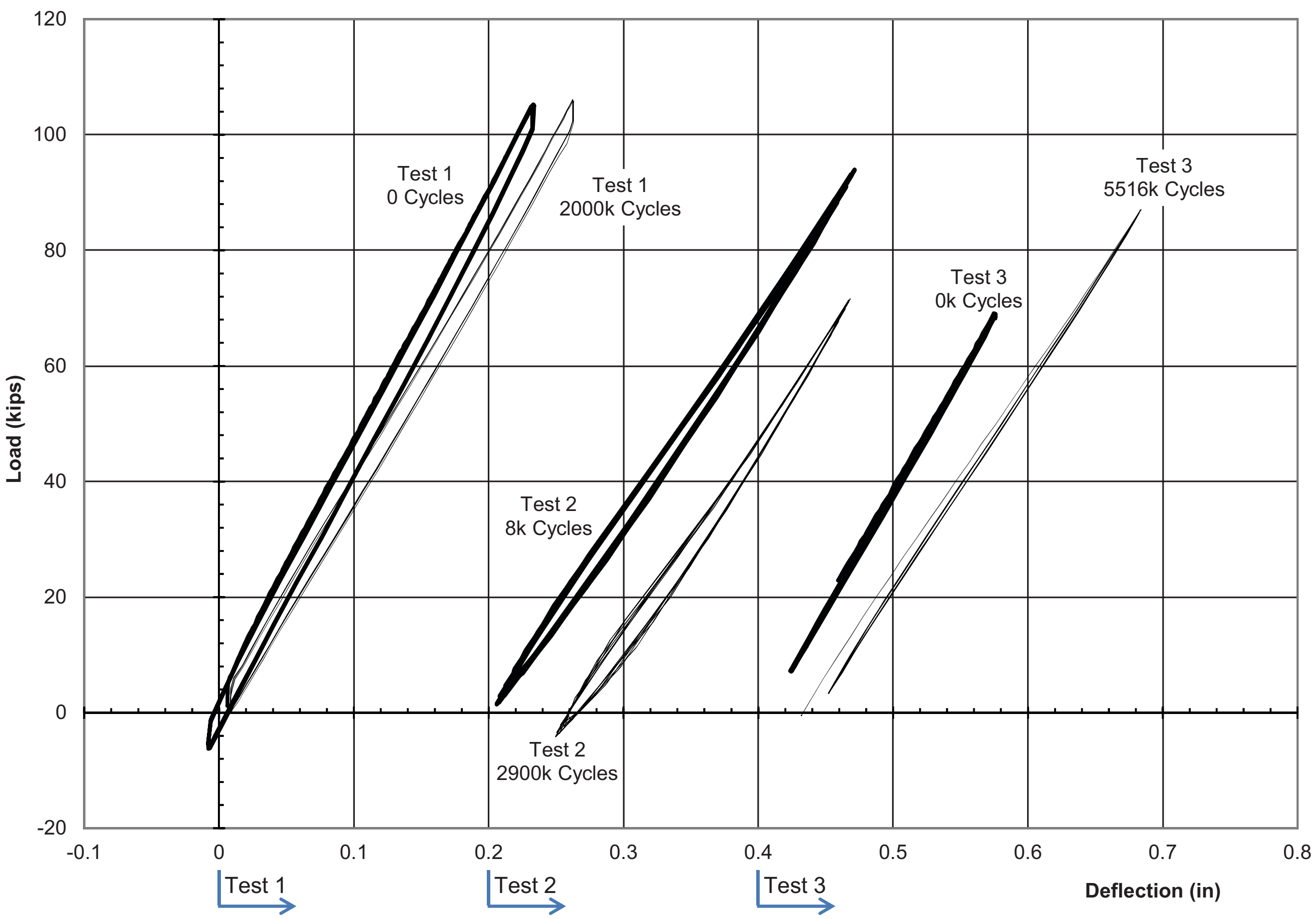

Fig. 8. Load-deflection plots of cyclic tests. The points of zero deflection for specimens 2 and 3 are shifted to the right to improve clarity.

softening in the load-deflection response of specimen 1 can be seen in Figure 9. The slope of the load-deflection curves at the zero cycle is about 437 kip/in. This slope decreased to about 394 kip/in. after 2,000,000 cycles. Figure 9 plots the resulting specimen stiffness over time. Because the adjustment was only needed once at 7400 cycles and there was virtually no change in specimen response throughout the remaining cycles, it is likely that the slight stiffness change was due to initial concrete damage, such as tensile cracking of the concrete deck. The loss of stiffness in test 1 was about 10% through the entire cycling test. The behavior of specimen 3 was very similar to that of specimen 1 and gave a similar stiffness value during the initial portion of loading. Several small adjustments were made at the outset of cycling to accommodate a small reduction in stiffness similar to that observed in specimen 1. After the load was increased, at 2,000,000 cycles, the stiffness did decrease slightly. Again, it is likely this decrease in stiffness was due to an initial finite amount of damage in the concrete, such as tensile cracking. Once the initial damage had taken place, the stiffness then stabilized and remained constant through the remainder of the test. The adjustments appear as permanent set in Figure 9.

The behavior of specimen 2 (test 2) was somewhat different than that observed in specimens 1 and 3. The actual initial stiffness of the structure is not accurately illustrated in Figure 9 due to the fact that the specimen was unable to support cyclic loading at the load level that was first applied. During the first portion of the testing, approximately 8000 cycles, the applied displacement had to be adjusted until the resulting load stabilized. The adjustments appear as permanent set in Figure 9. Note that the stiffness shown in Figure 9 is after 8000 cycles, when the specimen already had experienced a loss in stiffness; an elastic estimate of initial stiffness for specimen 2 would predict a value close to that of specimen 3 (test 3).

Vertical Strain Distribution

The vertical strain profiles through the depth of the diaphragm at the centerline of the pier are shown in Figure 10. These strains were measured by embedment gages inside the concrete diaphragm during the cycling tests. The strain distribution from both the specimens 1 and 3 (tests 1 and 3) exhibited only slight variations over the duration of the test. As evident in Figure 10, the strain distribution through the concrete diaphragm at the centerline is not linear, particularly in the case of specimen 3, in which the concrete must transfer the concentrated compressive load from the bottom flanges through the diaphragm. The magnitude of strains observed in both specimens 1 and 3 are similar, yet the load applied to specimen 1 was 25% greater.

The maximum observed compressive stress due to cyclic loading at the bottom of the diaphragm during test 3 was 2.2 ksi, which is 37% of the compressive strength of the material. The AASHTO LRFD specifications do not explicitly address the fatigue of concrete in compression; however,

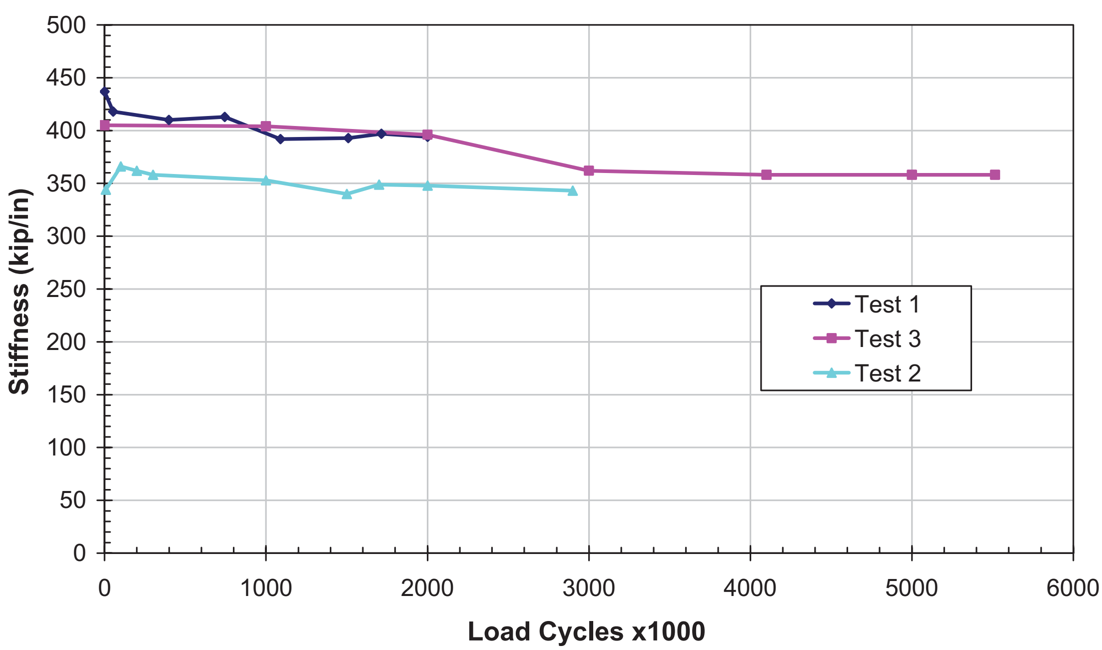

Fig. 9. Stiffness variation during cycling tests.

the observed stress level would satisfy the Eurocode provisions, which only require detailed investigation if the stress level is greater than 50% of the compressive strength (Milenkovic and Pluis, 2000).

Figure 11 shows a similar vertical strain profile for a section just outside of the diaphragm. As seen in Figure 11, the specimen 1 (test 1) strain profile remained virtually unchanged over the course of 2 million cycles. Although the profile obtained from specimen 3 (test 3) appears changed at the end of loading, recall that specimen 3 had an increase in the applied load after 2 million cycles. This increase in load would have the effect of scaling the strain values, resulting in a rotation of the strain profile, which is essentially what can be seen in Figure 11. Again, specimen 2 (test 2) is the exception, with a marked decrease in strains within the bottom flange by the end of the test.

The vertical distribution of the strain through the depth of the girder is not linear inside the concrete diaphragm (see Figure 11). This violates the assumption that plane sections remain plane in the classical beam theory, even though the concrete strain is within the elastic limit in the compression zone. However, the trend of the strain distribution outside of diaphragm is close to a linear fit. The one exception is specimen 2 (test 2), for which the bottom flange was observed moving relative to the concrete diaphragm. The nonlinearity of the strain profile for test 2 is additional evidence that the compression flange moved into the diaphragm. This movement was visible during the cyclic loading.

Strain in Deck Reinforcement

The strain in the deck reinforcement was also monitored during the fatigue loading for all three specimens. Figure 12 shows strain plots for the reinforcing bar located near the centerline of the deck in the top rebar layer (shown by an arrow in Figure 12). The longitudinal location of the gages was near the pier centerline. Care was taken in placing the reinforcement to ensure the single gage per bar was oriented toward the side of the bar to avoid localized bending effects. Additionally, longitudinal locations were chosen to avoid areas of large curvature to minimize local bending of the reinforcement, which can cause difficulties in strain measurements obtained with a single gage. During testing of specimen 1 (test 1), the tensile strain in the reinforcing steel varied only slightly over the 2 million cycles. In specimen 2 (test 2), there was a constant and significant increase of strain throughout the test, with the final value being nearly three times the initial value. In specimen 3 (test 3), there is an increase in the strain plot that coincides to the increase in applied load from 70 kips to 85 kips after 2 million cycles. Otherwise, there was little change. Note that the strains obtained for each specimen were in response to different load levels. The intent of Figure 12 is to show the change in strain over time of each individual specimen, not compare the absolute magnitude in the different specimens. For all specimens, the stress levels in the reinforcement remained below the threshold value required for infinite life according to the AASHTO LRFD specifications.

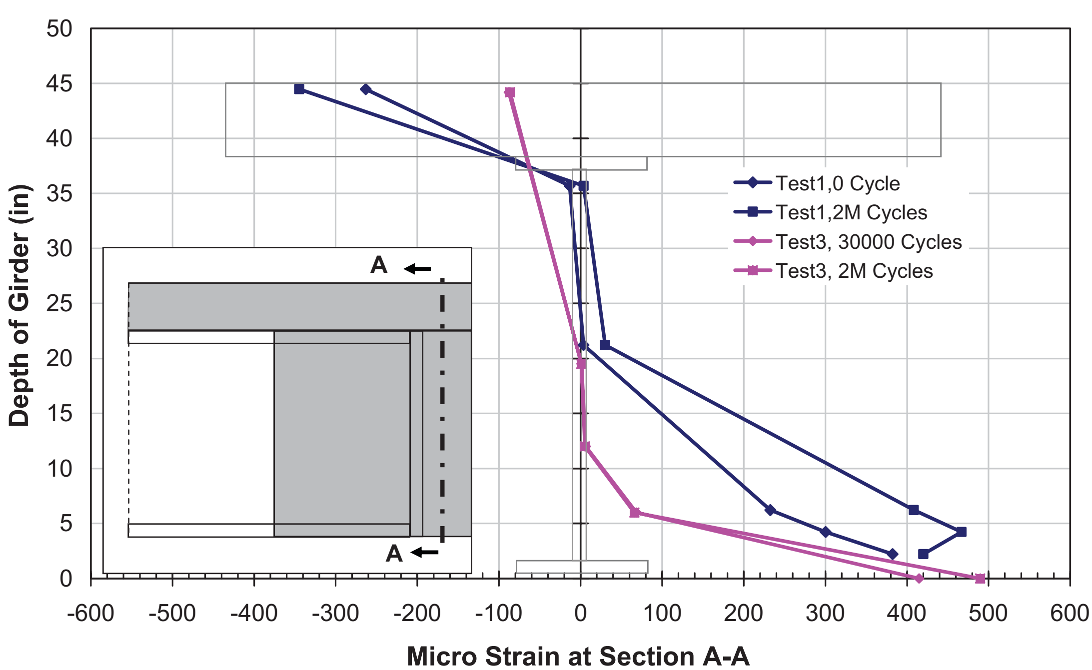

Fig. 10. Vertical profile of longitudinal strain at center of diaphragm.

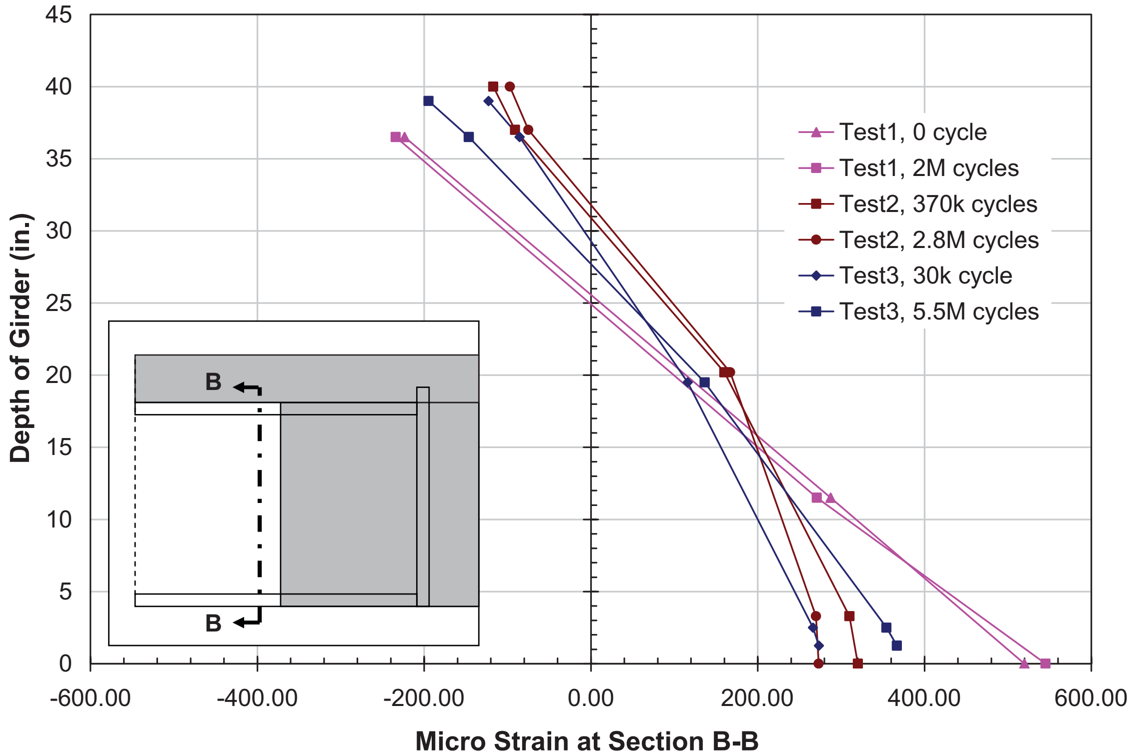

Fig. 11. Vertical profile of longitudinal strain outside of diaphragm.

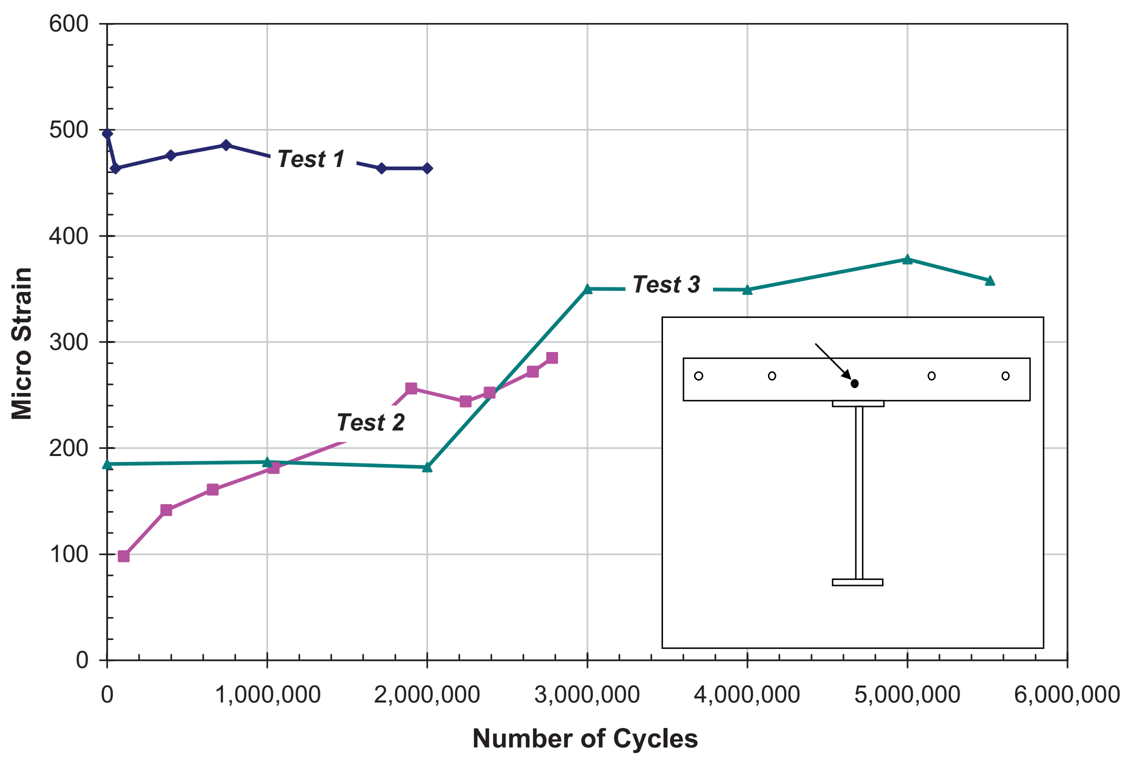

Fig. 12. Strain in top reinforcing bar.

ULTIMATE LOAD TESTING

The ultimate load tests were carried out to investigate the behavior of the specimen under ultimate load and evaluate the strength and ductility of the system. Loading of the specimen was applied through spreader beams placed on the deck at each end of the specimens. Threaded rods extended from the spreader to the basement of the structures laboratory. The loading system for the ultimate load test is shown in Figure 13. The distance from the spreader beam center to the centerline of the pier was 12 ft for specimen 1 and 15 ft for specimens 2 and 3. The change was necessitated by equipment constraints. During testing, displacement was applied in small increments with pauses for observations and data acquisition.

Results

The ultimate load tests were performed to obtain the ultimate load capacity of the various connections details and provide information regarding the associated failure mechanisms.

Load-Deflection

Load versus deflection plots were generated for both the west- and east-side cantilevers for each specimen. Because the location of applied load differed between the specimens, the loading data are expressed as moment and the deflection is normalized against the distance between pier centerline and load position. The responses from all three specimens have been combined in Figure 14. The saw-tooth appearance of the curve was caused by pauses for data collection, in which relaxation of the specimen occurs due to the onset of plastic flow. The maximum observed load, moment and deflection of the specimens are listed in Table 4. The values shown in the table refer to the maximum from either the west or east cantilever in each specimen. Notice that the moment capacities of the specimens 1 and 3 are approximately 1.5 times that of specimen 2.

From the data plot for test 1 (specimen 1), shown in Figure 14, it can be seen that the initially linear behavior ends near a moment of 3800 kip-ft. Further investigation into the experimental data revealed that the reinforcement near the girder centerline had just reached yield at this load. In

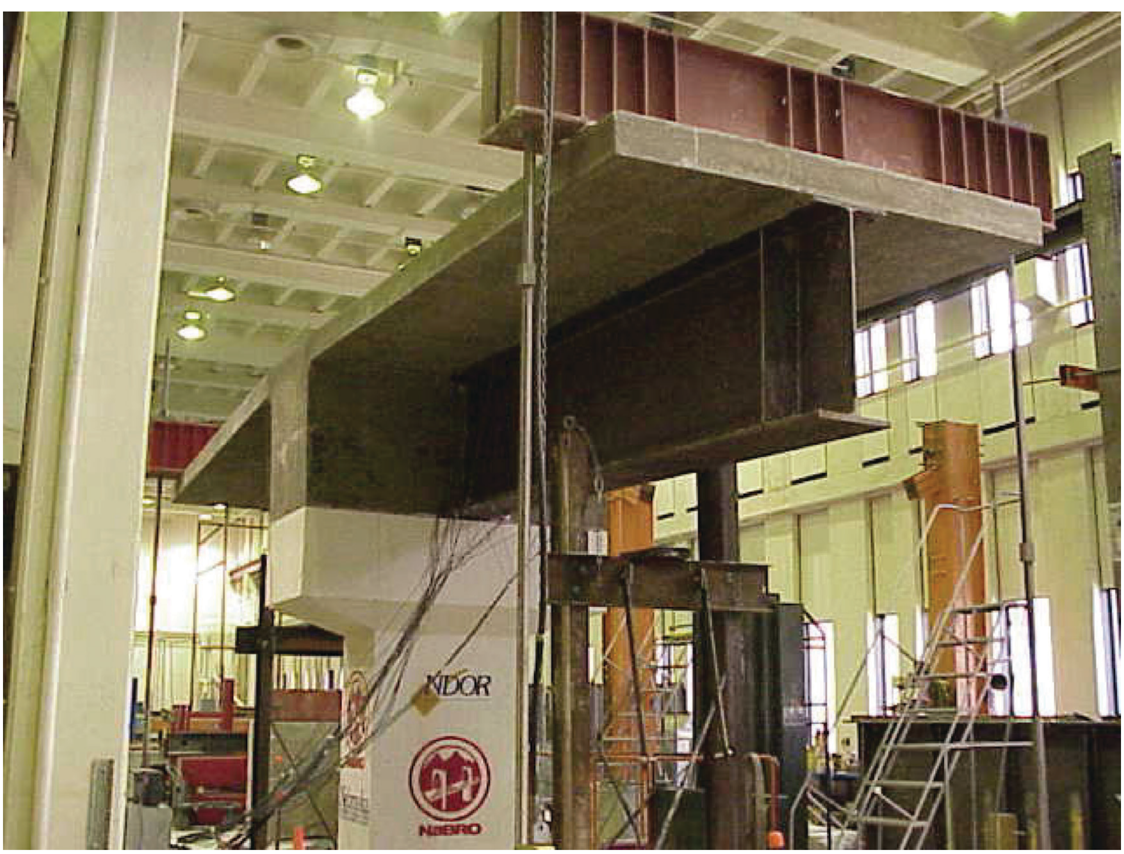

Fig. 13. Specimen 2 ultimate test setup.

Table 4. Displacement, Load and Moment at Maximum Observed Load			
Test	Displacement (in.)	Load (kip)	Moment (kip-ft)
1	2.59	516	6192
2	4.12	263	3945
3	4.50	391	5865

test 2 (specimen 2), the system response was linear up to a moment level of about 1800 kip-ft. At a moment magnitude of 3900 kip-ft, the system was unloaded due to a problem in the loading system. As a result of the initial loading, the system displayed a permanent set of approximately 0.75 in. Upon subsequent reloading, the system responded linearly until intersecting the original load-deflection curve. Despite substantial incurred damages, the initial stiffness during reloading was nearly equal to the original stiffness. The moment deflection behavior of test 3 (specimen 3) was quite similar to that of specimen 1. The initial elastic region ended at a lower load level of 1900 kip-ft. The loading rolled off smoothly until a load level of 5050 kip-ft, where a small break in the curve can be seen. The load level was still increasing slightly when the test was terminated due to the extreme deflection levels that were resulting in unsafe conditions in the load apparatus.

Cracking Observations

All specimens exhibited cracking of the concrete over the pier. As an example, cracking of specimen 3 is shown in Figure 15, which is representative of the general pattern of cracking displayed by all specimens. The results presented are for the ultimate loading. The cracking patterns are being used to interpret the failure modes. As such, the extent and magnitude of cracking are not indicative of what would be found at service levels. The following describes observations specific to each specimen.

Many of the cracks that initiated during the cyclic testing were simply widened in the ultimate test. At the end of the ultimate load test, cracks were observed penetrating through the depth of the slab at the edge of the diaphragm. There were both transverse and longitudinal cracks in the slab. The longitudinal cracks were found directly over the steel girder.

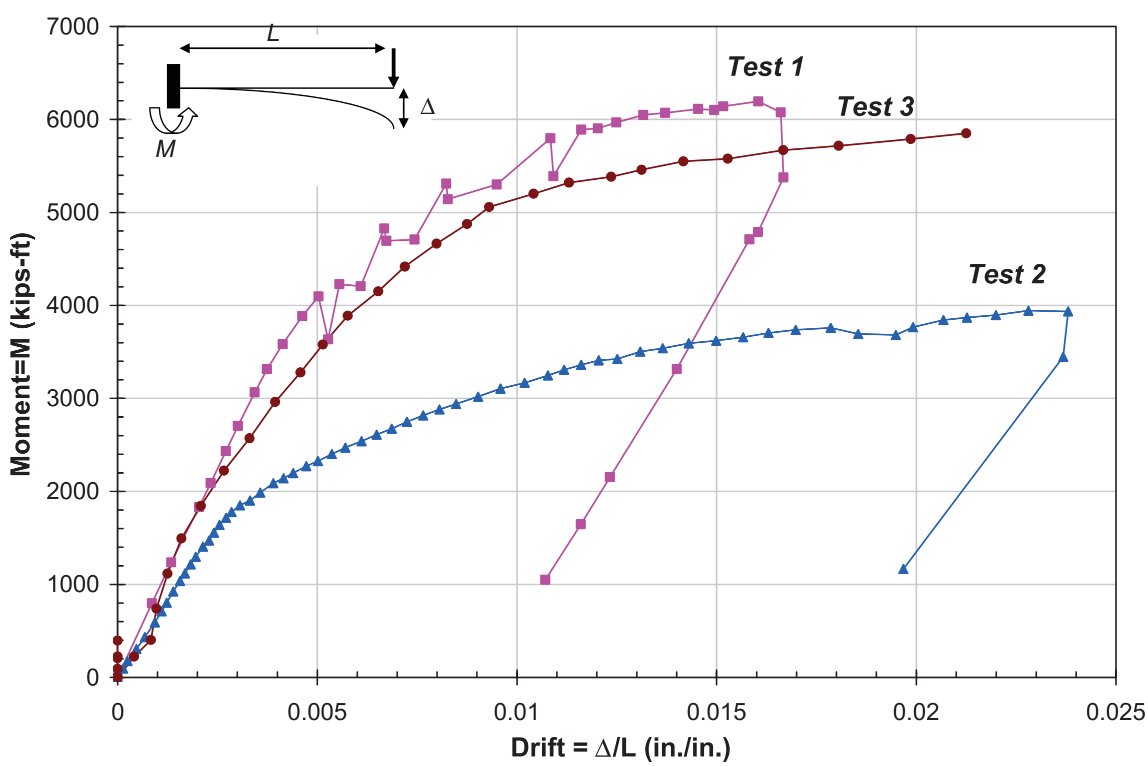

Fig. 14. Moment–drift plots of three experiments.

A 45° crack was observed at the diaphragm lateral face, indicating that cracking existed through the width of the diaphragm and had reached the outer face. This implies that the entire concrete diaphragm was participating in the resistance mechanism. No major cracks were observed around the bottom flange and the web.

From the outset of the ultimate load test for specimen 2, cracks in the concrete slab began to increase in width. Most of the cracks had formed during fatigue cycling, and these further increased in width during the ultimate load test. The majority of cracking occurred near the edge of the diaphragm. However, there were several large cracks at the centerline of the pier that were wider than those near the edge of the diaphragm. There were additional cracks through the depth of the slab. These cracks propagated further during the ultimate load test.

As was noticed in the previous specimens, the major cracks on specimen 3 were transverse and parallel to each other. These cracks penetrated through the depth of the slab. The 45° cracking at the lateral face of diaphragm was observed in this test as well. Cracks were also observed at the transverse face of the diaphragm initiating from the bottom flange toward the slab in approximately a 45° angle. As was noted for specimen 1, the inclined cracks on the lateral diaphragm face indicate that the failure of diaphragm concrete in these two specimens is not localized. This implies that the concrete diaphragm outside the width of the end plates (or outside the core concrete) participates in the ultimate strength of the connection.

Yielding of Longitudinal Reinforcement

Examination of strain values from specimen 1 indicate that the first yielding occurred in the top reinforcing layer near the girder centerline. This observation is a confirmation of one design goal during the initial specimen design, which was to achieve yielding of the tensile reinforcement prior to crushing of the bottom concrete (Lampe 2001).

Figure 16 shows the moment at the pier centerline when yield initiated in the top layer reinforcement for specimen 1. As can be seen, the middle bars yielded first or at a lower applied load than the outer bars. Load was then shed to adjacent bars as the loading continued. This is an illustration of the shear lag phenomenon in the concrete slab and the concept of effective width.

A similar result was observed in specimen 3. Unfortunately, strain data prior to load stage 24, which was beyond the initial yield point, were lost so the moment value at which initial yielding of the reinforcement occurred cannot be determined. However, the overall trend was observed in the available data, where strains in the middle bars were above yield and significantly higher than the strains in the gages near the edges.

Behavior of specimen 2 was different in that only two of the reinforcing bars were observed to yield prior to failure of specimen. However, similar to the pattern observed in tests 1 and 2, both of these bars were located near the centerline of the deck. The outer bars remained in the elastic region throughout the loading of specimen 2.

Observed Ductility of Connections

The observed ductility of the connections is defined as the displacement at the maximum applied load, or displacement at completion of the test if load is still increasing, divided by the deflection of the first yield in the system. Based on this definition, the observed ductility ratios of the three specimens are given in Table 5. In this table, the first yield load

(a)

(b)

Fig. 15. Specimen 3 crack patterns at completion of ultimate test: (a) concrete slab, plan view; (b) face of diaphragm.

Table 5. Yield Load, Displacements and Ductility Ratios				
Specimen	First Yield Load (kips)	Yield Displacement (in.)	Displacement at Maximum Load (in.)	Observed Ductility Ratio
1	320	0.66	2.59	3.92
2	191	1.54	4.12	2.67
3	290	1.45	4.50	3.10

of specimen 3 was interpolated based on the first yield load of specimen 1 and the yield load obtained from the only strain gage functional in the top layer of specimen 3. Note that specimen 1 has the maximum observed ductility while specimen 2 has the minimum.

Behavior of Concrete in Compression Zone

Strains from specimen 1, recorded by embedment gages placed inside the diaphragm between the two girders, are shown in Figure 17. The elevations given are measured from the top of the bottom flange to the gage. Also shown in the figure are strain values obtained from a gage attached to the top of the bottom flange. Note that the embedment gages are not capable of measuring strains above 1800 micro-strain, which is less than the typical failure strain of the concrete (3000 micro-strain). As shown in Figure 17, the bottom plate strain gages passed the 3000 micro-strain at load level of 450 kips.

In specimen 2, crushing of the concrete was evident during the cycling test, and by the end of the ultimate test, the gap between the bottom flanges had reduced from the initial separation of 8 in. to 5 in. (see Figure 18).

Although the embedment gages directly in line with the girders were compromised, those only a short distance away measured relatively small strains during the ultimate test. This indicates that the concrete damage was highly localized around the interface of the bottom flange and the diaphragm. Essentially, the web and bottom flange of the steel girder acted like the edge of a knife that cut through the concrete diaphragm.

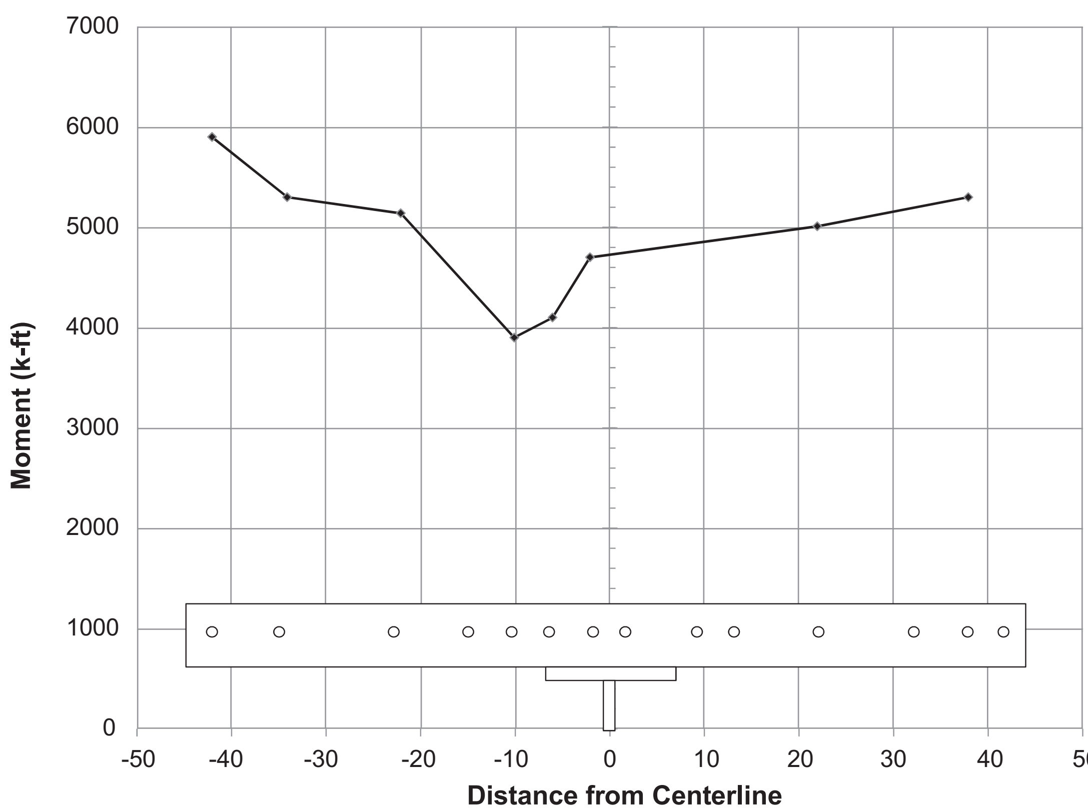

Fig. 16. Moment at which yield initiated in the top layer rebar—specimen 1.

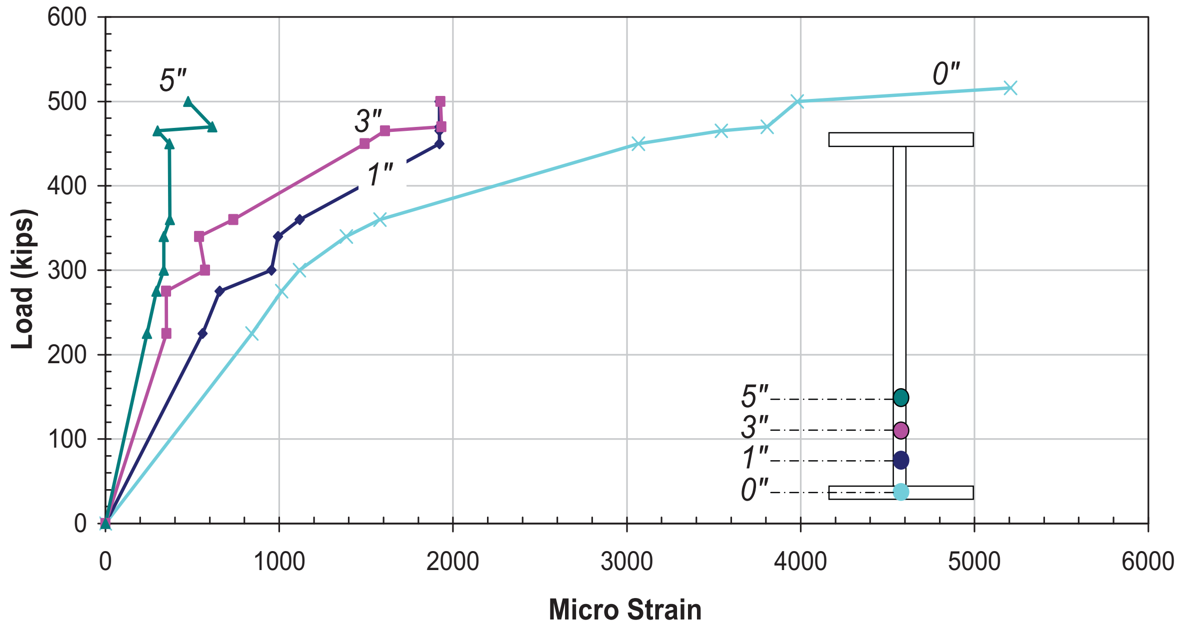

Fig. 17. Strain in concrete diaphragm between girders—specimen 1.

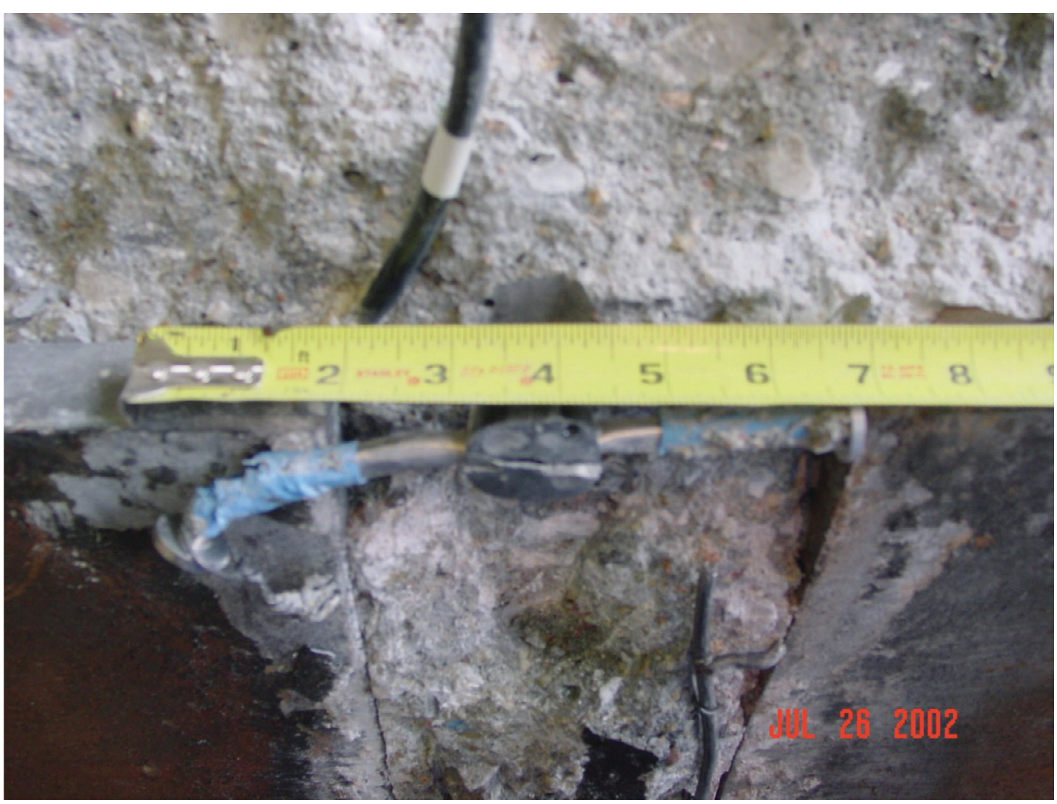

Fig. 18. Gap between bottom flanges.

In specimen 3, many of the embedment gages between the two bottom flanges were no longer functioning by the start of the ultimate test. It is unclear if this was due to damage of the gages as a result of excessive strains or damage to the wiring, either of which could have been sustained during cyclic loading. A few gages located farther from the bottom flange survived and measured the concrete strain throughout the test. The load-strain plots of two embedment gages placed at the centerline of the pier are shown in Figure 19. The strain reading of EG-10 exceeded the typical crushing strain of concrete (3000 micro-strain). Note that this was a different gage type than was used on specimen 1, which could only read up to 1800 micro-strain. Therefore, the concrete in vicinity of this gage and at the lower depths would be expected to have crushed. Instrumentation monitoring movement of the steel girder relative to the face of the diaphragm indicates that the steel pushed into diaphragm 0.35 in. on each side, which would also support the conclusion that the concrete had crushed by the end of the test.

Strain Distribution through the Depth

The strain distribution through the depth of the section has a crucial role in determining the resistance mechanism of the system. Figure 20 shows the strain profile at three different locations within and near the diaphragm. The values reported are from a time when the applied load was near the maximum observed value. Values for each section were not available for all specimens. The strain distribution inside the concrete diaphragm and at the centerline of the pier for specimen 1 is shown in Figure 20a. Due to high compressive stress in this region, most of the embedment gages placed inside the diaphragm of specimens 2 and 3 failed during the ultimate tests. As seen in Figure 20a, the strain distribution at the centerline of the pier inside the diaphragm is not linear but rather exhibits deep beam behavior where plane sections do not remain plane during loading. A plot of the vertical strain profile has been repeated in Figure 20b for a section that is still inside the diaphragm but away from the pier centerline. Here, data are available both from embedment gages indicating strains in the concrete and gages on the steel girder indicating the strains in the steel section. Again, some degree of nonlinearity is observed in the strain profile. Specifically, note the embedment gages near the bottom of the profile.

Finally, the strain distribution obtained from all three tests at a section outside of the diaphragm is depicted in Figure 20c. In this case, the strain profile is much closer to a linear pattern than the previous cases. In both Figures 20b and 20c, the large strains in the steel at the top of the section are due to yielding of the steel. The variation of strain along the

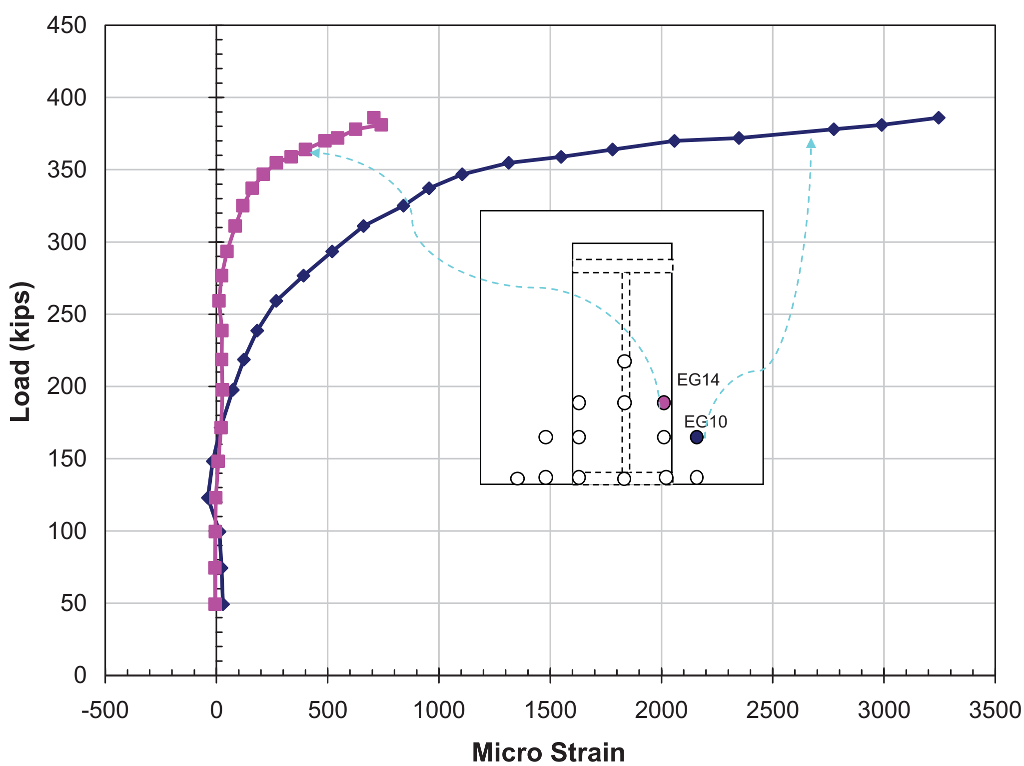

Fig. 19. Strain in concrete diaphragm between girders—specimen 3.

depth of specimen 3 is very close to specimen 1 behavior. It is noted that the applied moment at this section is approximately equal for specimen 1 and specimen 3. These plots indicate that the assumption that the plane sections remain plane can be justified for the steel girder strain profile but not within the concrete diaphragm.

Strain Distribution along the Length of the Flanges

The strain responses along the length of the flanges for the three specimens are shown in in Figure 21. The strain values shown are for when the loading was near the maximum observed value. The strain in the bottom flange, inside the core, of specimen 1 (test 1) exceeded the yield limit of the steel. Yielding was not observed in the other two specimens (test 2 and test 3) at the bottom flange. As seen in this figure, the strain reached a maximum value near the intersection of the bottom flange and the end bearing plate in test 1. The reduction of the strain within the core diaphragm could be due to the compressive resistance of the concrete sharing a portion of the compressive force with the bottom flange. This contribution from the concrete can also be seen in the strain profile from specimen 3. The decrease in bottom flange strain within the diaphragm compared to outside of the diaphragm can be attributed to composite action of the concrete diaphragm and steel girder. Bottom flange strain data from inside the diaphragm for specimen 2 were not available.

Next consider the top flange strain profile shown in Figure 21. Note that the strain values drop substantially near the end of the top flange. These low values are expected because the concrete that is immediately beyond the tip of the top flange cannot transfer the tension force. The spikes in the top flange strain at the face of the diaphragm seen in specimens 2 and 3 are likely due to concentrated rotation (kink) at the face of the diaphragm (the gage is on the top of the top flange). Further evidence of the concentrated rotation is the degree of cracking observed in the deck at this location, as discussed previously.

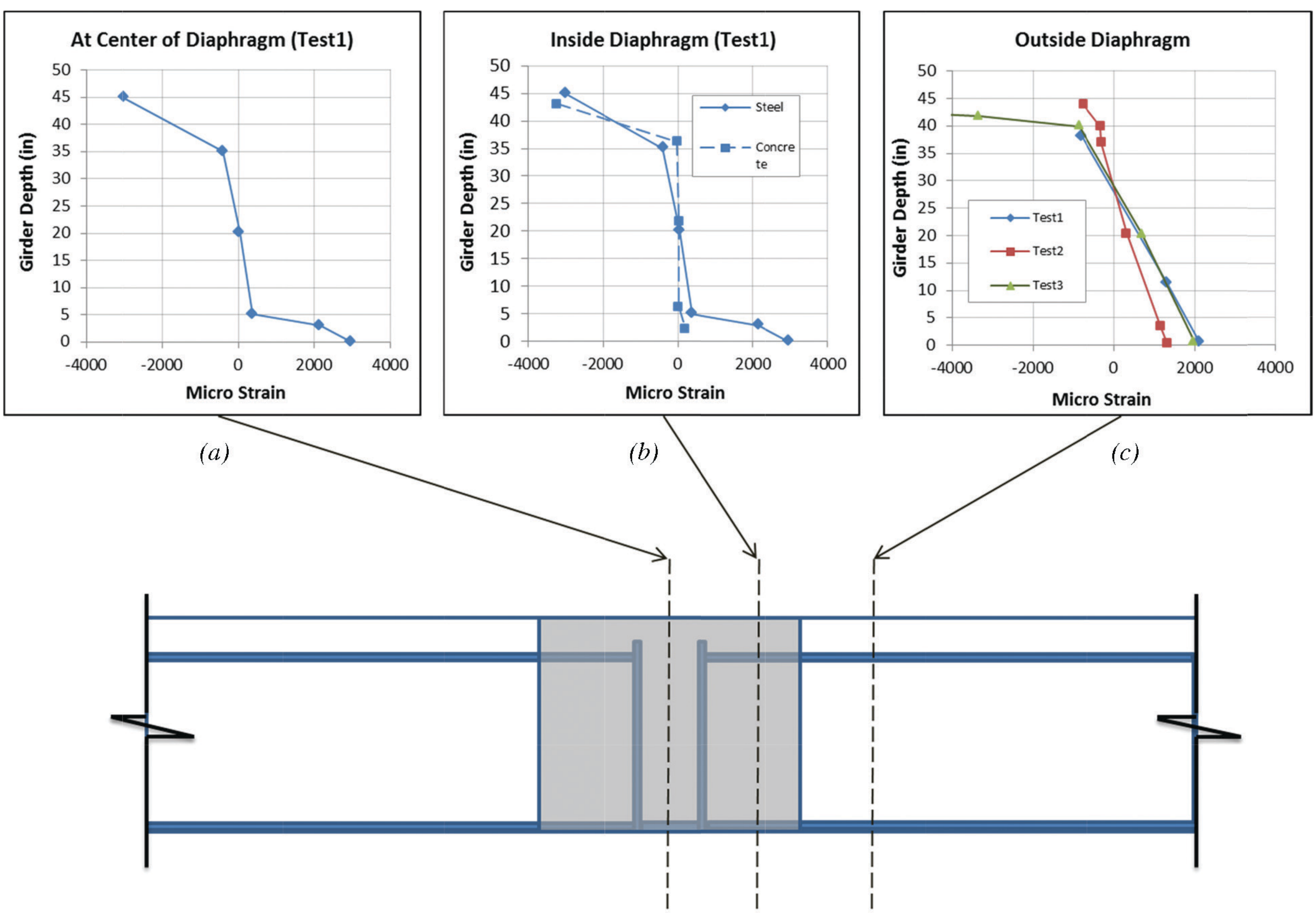

Fig. 20. Vertical strain profiles at maximum load condition.

Interface Behavior between Steel Girder and Concrete Diaphragm

The girder end detail used in specimen 1 was intended to divert compressive force away from the diaphragm concrete. Specimen 3 utilized end plates to distribute the compressive force over an increased concrete area. Specimen 2 allowed the concentrated compressive force from the steel to be applied over the steel girder area only. In addition to direct bearing, the compressive force was also transferred by bond between the portion of the girder that was embedded in the diaphragm and by transverse steel bars within the diaphragm that passed through holes in the girder web.

In specimen 2, penetration of the bottom flange into the diaphragm, along with the formation of large cracks (see Figure 22) indicates that bonding between the steel girder and concrete diaphragm failed during testing of specimen 2. After conclusion of the ultimate test, the dissection of specimen 2 revealed that the transverse bars placed through holes in the web had been sheared through, as shown in Figure 23. Recall this specimen was deliberately intended to illustrate the failure mechanisms of simplistic detail and the shearing of reinforcement was not observed in specimens 1 and 3.

The connectivity of the top flange and the concrete slab was ensured by designing and providing an adequate number of shear studs on the top flange. The visual observation of the studs after conclusion of the ultimate tests and dissections of the specimens did not show failure of the studs.

Summary of Observed Behavior

The test results presented in the preceding sections are summarized to give a general picture of the behavior of the test specimens. For each specimen, the load corresponding to the theoretical plastic moment is given. This calculation is

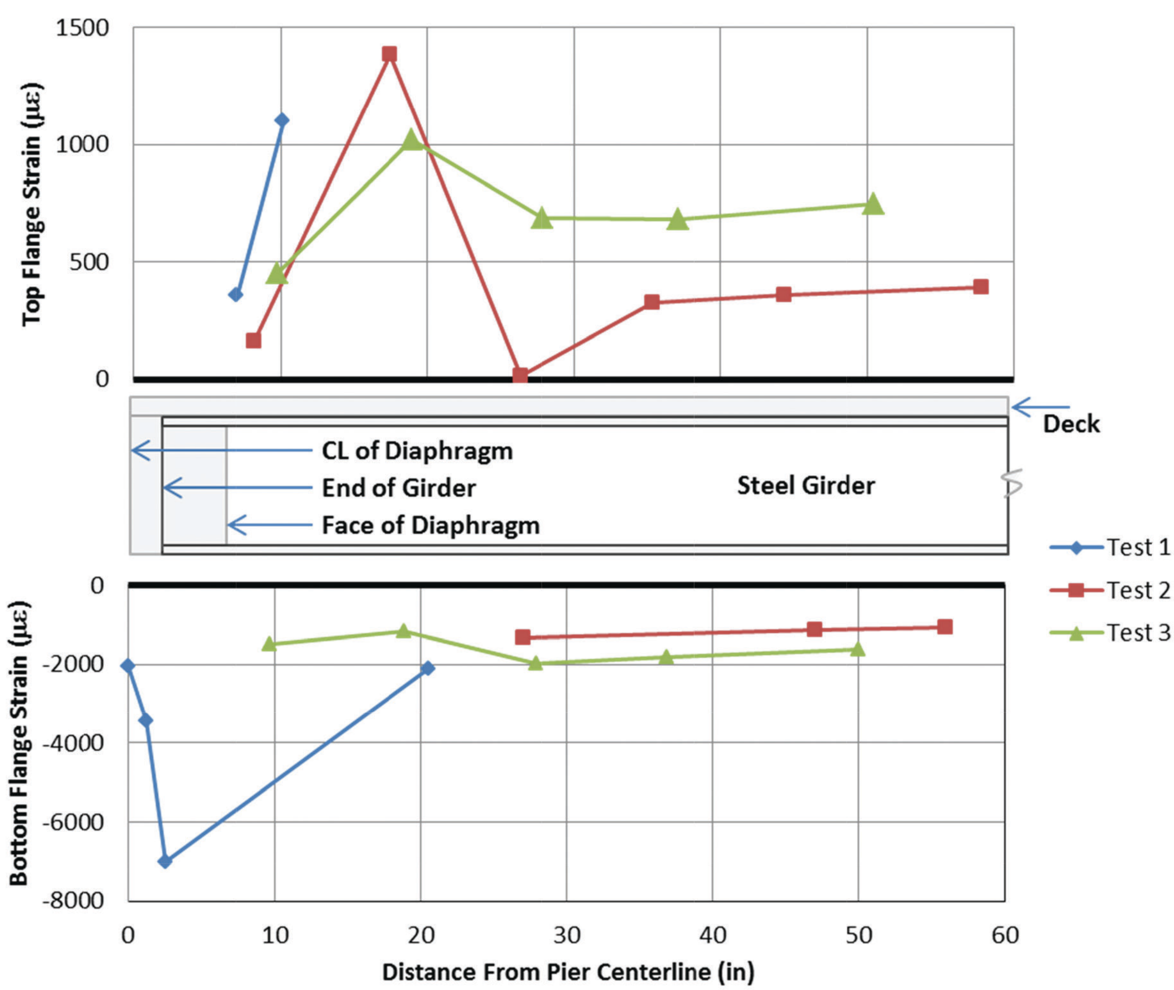

Fig. 21. Strain profile along the longitudinal axis of both flanges.

based on the actual material properties and assumes complete participation of the full steel section and reinforcement. The assumption provides a value for reference and is not necessarily a basis for strength calculation, which is discussed in more detail elsewhere (Farimani et al., 2013). The arm distance for calculating the applied moment is taken to the center of the diaphragm and was 12 ft for test 1 and 15 ft for tests 2 and 3.

Specimen (Test) 1

Behavior of specimen 1 during ultimate load test is shown in Figure 24. The load corresponding to the theoretical plastic moment calculated at the face of the diaphragm is 510 kips. This figure identifies several important stages during ultimate load test. Each of the events identified in Figure 24 is described here:

1. The cracks remaining from the cycling test widened and propagated in the concrete slab from the early stage of loading (5% of the maximum observed load). These cracks started at the diaphragm edge and the centerline of the pier.
2. The yielding started at the top layer of reinforcements at 62% of the maximum observed load. The location of the first yield was around the girder axis and centerline of the pier.
3. After a further small increase in load to 65% of the maximum observed load, the bottom plate strain passed the yielding limit.
4. The concrete between the two end bearing plates at the bottom of the diaphragm experienced strain more than 0.003 in./in. at 87% of the maximum observed load.
5. The entire top layer rebar passed the yielding limit at 95% of the maximum observed load.
6. All of the slab rebar around the pier centerline yielded at 98% of the maximum observed load.

Specimen (Test) 2

The load-deflection response of specimen 2 is shown in Figure 25. The deflection values in the plot are average values obtained from the readings of the east and west girders. The load corresponding to the theoretical plastic moment calculated at the face of the diaphragm is 414 kips. The maximum applied load was well below this value. Due to damaged instrumentation, there were not adequate data to quantify the structural behavior of the system as were obtained for specimen 1. However, based on the visual observations along with the recorded data, the behavior of the system is predicted as follows:

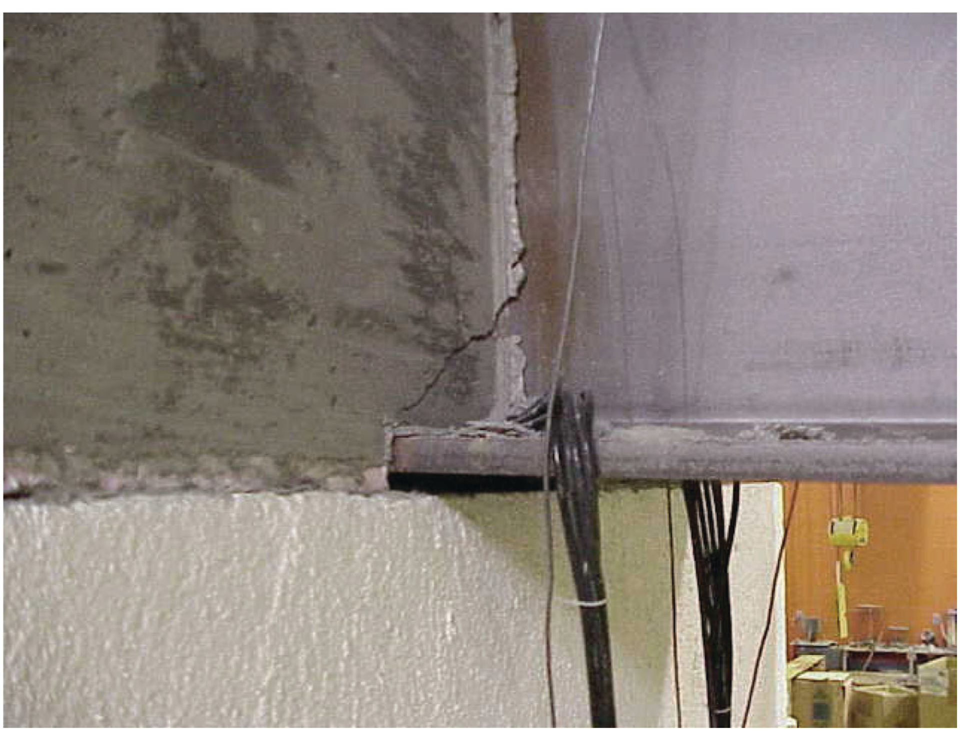

Fig. 22. Cracking of the concrete diaphragm around the bottom flange—specimen 2.

1. The cracks formed during the cycling loads grew from beginning of loading, especially on the surface of deck.
2. Local crushing of concrete occurred at the interface of the bottom flange and the concrete after cracking, but there are not enough data to locate more exact load level.
3. The large deformation and failure of the transverse reinforcement within concrete diaphragm occurred at 43% of the maximum observed load.
4. At 78% of the maximum observed load, the first bar at the middle of the top layer at the pier centerline yielded.
5. The slab concrete around the top flange and edge of diaphragm failed at about 97% of the maximum observed load.

It is noted that the bond between the steel girder and the concrete diaphragm failed during the cycling test and so has not been shown here. The failure of the specimen occurred following the failure of the concrete deck. Movement of the beam bottom flanges (compression flange) into the concrete diaphragm resulted in large rotation of the steel girder and pull out of beam top flange (tension flange) from the concrete diaphragm, as shown in Figure 26.

Specimen (Test) 3

The load-deflection response of specimen 3 is shown in Figure 27. This figure is the average of the east and west girders. The load corresponding to the theoretical plastic moment calculated at the face of the diaphragm is 412 kips. The exact location of the structural events for this test, similar to that described for test specimen 1, was not possible due to loss of instrumentation. However, test observations and results indicate that the resistance of the specimen is predicted as follows:

1. Concrete cracks formed during the cycling test propagated from the beginning of the ultimate test.
2. The first yield would be estimated at about 60% of the maximum observed load.
3. The top rebar layer yielded at 80% of the maximum observed load and caused the slope of the load-deflection plot to change around this point.
4. The failure of the specimen occurred as inclined cracks formed throughout the concrete diaphragm.

Fig. 23. Shear failure of the transverse bar inside the diaphragm after the conclusion of the ultimate test—specimen 2.

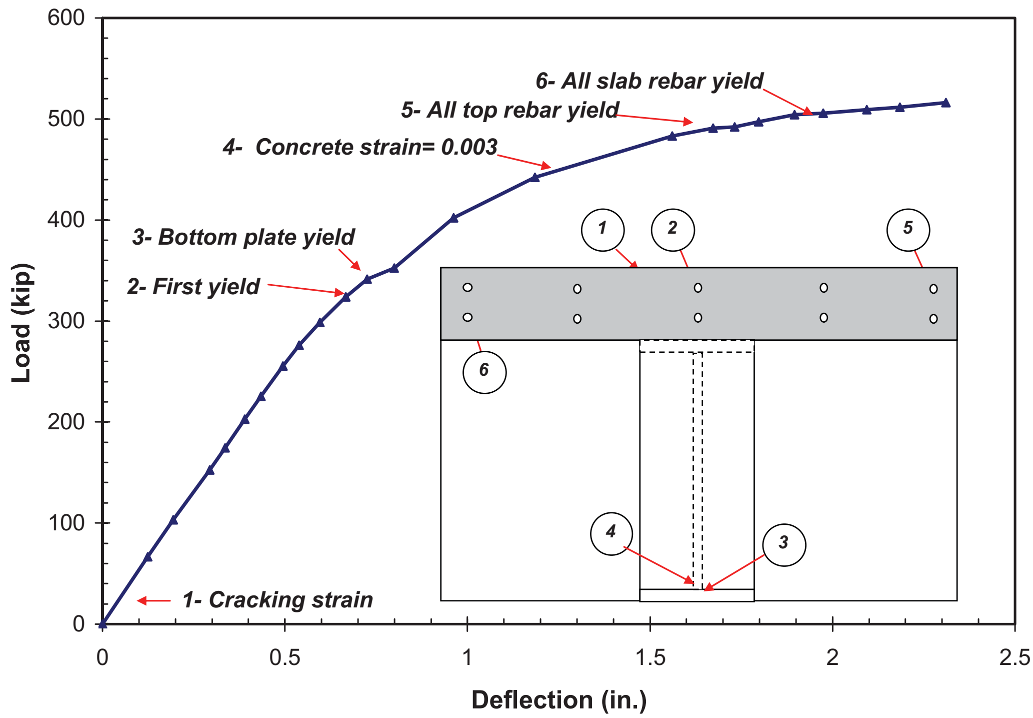

Fig. 24. Specimen 1 observations.

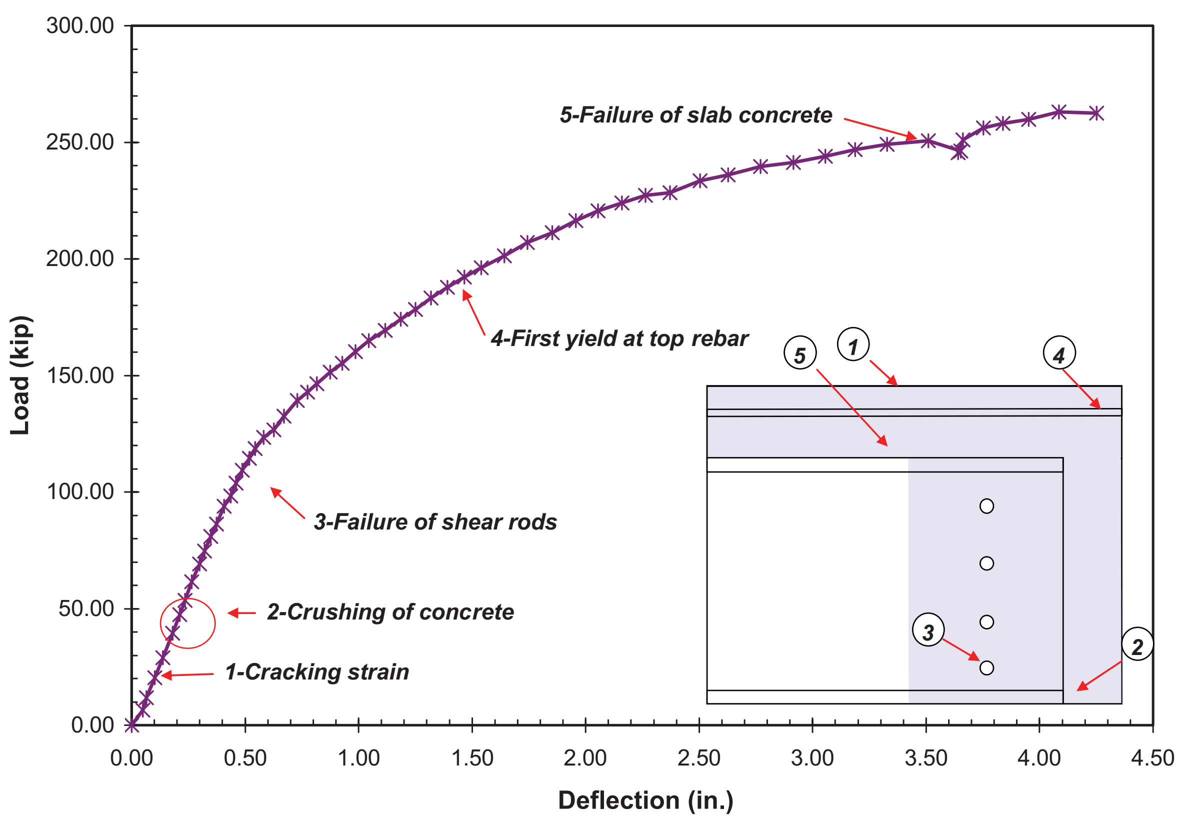

Fig. 25. Specimen 2 observations.

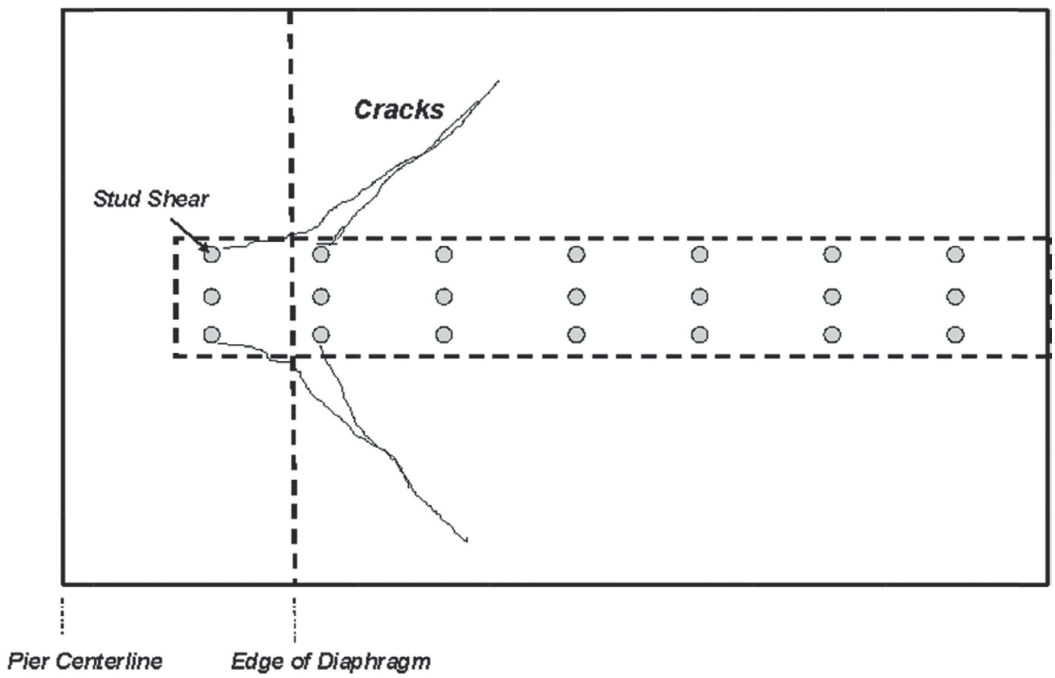

Fig. 26. Concrete failure of the specimen 2 deck.

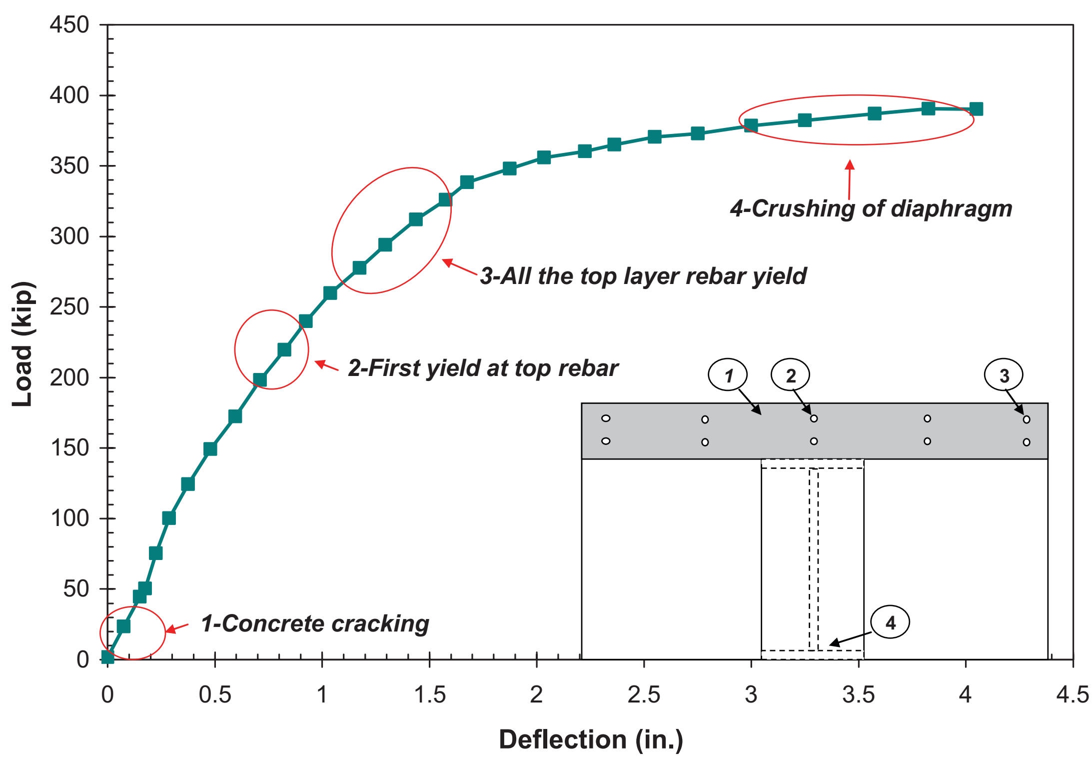

Fig. 27. Specimen 3 observations.

CONCLUSIONS

The compressive force component, carried by the bottom flange, should not be transferred directly to the concrete at the interior support. It is preferred that a continuous steel path be provided for the compressive force, such as that provided by the detail used in specimen 1. Note, however, that the detail in specimen 1 was intended to be proof-of-concept detail but is not necessarily practical for field implementation.

Test 2 showed that the compressive force is sufficiently concentrated and crushing of the concrete can occur, thus necessitating the force transfer through a steel path. The ultimate performance of specimen 3, which utilized an end plate to distribute the load, was comparable to that of specimen 1, with a continuous steel path. However, there were some differences in the observed data during the cyclic testing. For this reason, the end plate detail is not recommended at this time, though it may actually provide satisfactory performance. Instead, a mechanism should be provided to prevent transfer of compression force from the bottom flanges to the concrete diaphragm. One practical detail that provides a continuous steel path, but is simpler to construct than the detail used in specimen 1, is shown in Figure 28.

The specimens were designed following the concepts from reinforced concrete that prevent over-reinforcement of the system. This requires that sufficient compressive resistance should be developed to force initial yield to occur in continuity reinforcement within the slab. This was achieved in both the specimens 1 and 3. Specimen 2 did not possess sufficient compressive resistance to cause yield in the continuity reinforcement.

The maximum applied load for specimen 1 exceeded the load corresponding to the theoretical plastic moment capacity obtained, assuming full participation of the steel section. The maximum applied load for specimen 2 was well below the plastic capacity, and the maximum applied load for specimen 3 was just below the plastic capacity.

One of the primary conclusions is that experimental testing confirmed that reinforcement in the deck is sufficient to develop continuity. That is, the top flange does not need to be made continuous over the interior support. The extent of the cracking observed during the cyclic testing was minimal and comparable to what is expected in conventionally detailed construction, even at the amplified load levels that were used, such that no durability issues are expected.

The results of the three tests that were conducted provide good insight into the resistance mechanism at work in the system, but due to limited experimentation, a general mechanism cannot be derived from experimentation alone. Furthermore, the results from the three specimens do not provide enough data points to adequately quantify the ultimate capacity of the structure. To obtain more information regarding the behavior of system, a series of finite element analyses were completed to compliment the experimental studies. The numerical studies are presented in Farimani et al. (2014).

ACKNOWLEDGMENTS

The initiative was directed by Atorod Azizinamini, Professor and Chair at Florida International University, and was made possible by contributions from many current and former graduate students and research associates, as well as input from many in the bridge community. In particular, the contributions of the following individuals are acknowledged.

Graduate students earning degrees from the project were Nick Lampe, Nazanin Mahasebi, Reza Farimani, Saeed Javidi, Derek Kowalski and Mark Otte. The research study

Fig. 28. Bearing block detail.

was conducted at the University of Nebraska–Lincoln. Aaron Yakel was the research associate assisting the project. Laboratory technicians Jeff Boettcher, John Dageford, and Peter Hilsabeck assisted in conducting the experimental portion of the study. Graduate students who assisted with experimental testing include John Swendroski, J. Brian Hash, Patrick Mans, Luke Glaser and Nima Ala. The study was supported by the Federal Highway Administration and the Nebraska Department of Roads. Several visionary engineers at NDOR were critical to the successful completion of the project: Lyman Freeman, Moe Jamshdi and Hussam "Sam" Fallaha. Steel fabrication and assistance during specimen preparation were provided by Capitol Contractors of Lincoln, NE.

The opinions and conclusions presented in this paper are those of the authors and do not necessarily represent the viewpoints of the project sponsors.

REFERENCES

AASHTO (1998), *LRFD Bridge Design Specifications*, 2nd Ed., American Association of State Highway and Transportation Officials, Washington, DC.

Azizinamini, A. (2014), "Simple for Dead Load–Continuous for Live Load Steel Bridge Systems," AISC, *Engineering Journal*, Second Quarter.

Azizinamini, A., Lampe, N.J. and Yakel, A.J. (2003), *Toward Development of a Steel Bridge System—Simple for Dead Load and Continuous for Live Load*, A Final Report Submitted to the Nebraska Department of Roads, National Bridge Research Organization: www.nlc.state.ne.us/epubs/r6000/b016.0088-2003.pdf.

Azizinamini, A., Yakel, A.J., Lampe N.J., Mossahebi, N. and Otte, M. (2005), *Development of a Steel Bridge System—Simple for Dead Load and Continuous for Live Load, Volume 2: Experimental Results*, Final Report NDOR P542, Nebraska Department of Roads, Lincoln, NE.

Farimani, M.R., Javidi, S.N., Kowalski, D.T. and Azizinamini, A. (2014), "Numerical Analysis and Design Provision Development of the Simple for Dead Load–Continuous for Live Load Steel Bridge System," AISC, *Engineering Journal*, Second Quarter.

Milenkovic, A. and Pluis, M. (2000), "Fatigue of Normal Weight Concrete and Lightweight Concrete," European Union—Brite EuRam III, Document BE96-3942/R34.

Mossahebi, N. (2004), *New Steel Bridge System: Simple for Dead Load, Continuous for Live Loads*, M.S. Thesis, University of Nebraska–Lincoln, Lincoln, NE.

Lampe, N.J. (2001), *Steel Girder Bridges Enhancing the Economy*, M.S. Thesis, University of Nebraska–Lincoln, Lincoln, NE.

Szerszen, M.M. and Nowak, A. (2000), "Fatigue Evaluation of Steel and Concrete Bridges," *Transportation Research Record,* Vol. 1696.